PLANETARY NEBULAE AS STANDARD CANDLES X. TESTS IN THE COMA I REGION

George H. Jacoby
Robin Ciardullo
William E. Harris

NOAO Preprint No. 675

Accepted by: *The Astrophysical Journal*

October 1995

Planetary Nebulae As Standard Candles X. Tests In The Coma I Region

George H. Jacoby
Kitt Peak National Observatory, National Optical Astronomy Observatories, P.O. Box 26732, Tucson, AZ 85726

and

Robin Ciardullo[1,2]
Department of Astronomy and Astrophysics, Penn State University, 525 Davey Lab, University Park, PA 16802

and

William E. Harris[1]
Department of Physics and Astronomy, McMaster University, Hamilton, Ontario, Canada L8S 4M1

---

[1]Visiting Astronomer, Kitt Peak National Observatory, National Optical Astronomy Observatories, which is operated by the Association of Universities for Research in Astronomy, Inc., under cooperative agreement with the National Science Foundation.

[2]NSF Young Investigator

ABSTRACT

We present the results of an [O III] λ5007 survey for planetary nebulae (PN) in three galaxies of the Coma I group: NGC 4278 (Hubble type E1), NGC 4494 (E1), and NGC 4565 (edge-on Sb). Using the planetary nebula luminosity function (PNLF), we derive distances to NGC 4494 (12.8 ± 0.9 Mpc), NGC 4565 ($10.5^{+0.8}_{-1.0}$ Mpc), and NGC 4278 ($10.2^{+0.7}_{-1.0}$ Mpc). The larger distance for NGC 4494 is significant beyond the 99% confidence level when the common systematic errors in all 3 distances are removed. This agrees with the results of the globular cluster luminosity function and surface brightness fluctuation methods, both of which place NGC 4565 in front of NGC 4494. The large separation is also consistent with the results of Virgocentric flow models, which predict triple valued solutions to the Hubble flow in that direction.

Our planetary nebula survey of the small elliptical NGC 4278 also reveals two [O III] λ5007 sources more luminous than the nominal limit of the PNLF. Both objects can be excluded *a priori* from the list of PN candidates: one is quite bright in Hα, the other is marginally resolved. Nevertheless, the existence of these objects in an otherwise normal elliptical galaxy poses a potential problem for the PNLF technique. We discuss the possible origins of objects brighter than the PNLF cutoff, and consider one way in which their existence might be incorporated into PNLF distance measurements.

Subject headings: distance scale — galaxies: clusters — galaxies: distances — nebulae: planetary

1. INTRODUCTION

The acceptance of any extragalactic distance indicator demands that it be tested for the presence of systematic errors. One of the simplest of these errors to understand may occur when viewing galaxies with differing Hubble types. An indicator that works within a spiral galaxy may not necessarily work the same way in an elliptical, due to differences in the underlying stellar population or mass distribution. Evidence for such an effect has been seen in the magnitudes of Type Ia supernovae (Hamuy *et al.* 1995) and for the globular cluster luminosity function (GCLF; Fleming *et al.* 1995). Since distance indicators such as the GCLF, the planetary nebula luminosity function (PNLF), surface brightness fluctuations (SBF), novae, and Type Ia supernovae are all used in early-type galaxies, but calibrated in spirals (via Cepheids), it is exceedingly important that tests for systematic errors of this type be performed.

There are two ways to search for such biases. The first technique is purely internal: distance estimates can be made to elliptical and spiral galaxies within a common, compact group. As long as there is no morphological segregation, an error-free indicator will yield similar distances to both

types of galaxies. Since spiral galaxies are not always intermixed spatially with ellipticals, this test may occasionally yield a false result. However, if enough galaxy groups are analyzed, then the effects of morphological segregation should be reduced statistically.

The second method for detecting systematic distance errors is through external comparisons with the results of other methods. If the residuals between one distance indicator and another show a systematic trend with Hubble type, then it is likely that at least one of the methods is biased. Since no distance indicator is perfect, comparisons of this kind must assume that the errors of one method are uncorrelated with those of the other. Fortunately, this is usually a good assumption, especially since the physics underlying the most popular distance indicators are vastly different from one another (cf. Jacoby *et al.* 1992).

In this paper, we use a nearby, well-mixed group of galaxies in Coma I to examine the PNLF method for the presence of a spiral–elliptical systematic error. This group has long been recognized as a fertile proving ground for distance indicators, as it contains several spiral and E/S0 galaxies within a $\sim 1.8 \times 0.8$ Mpc elliptical region (de Vaucouleurs 1975). Moreover, two of the galaxies in the group, the E1 galaxy NGC 4494 and the giant edge-on spiral NGC 4565, have recently been measured with the SBF (Simard & Pritchet 1994) and GCLF (Fleming *et al.* 1995) techniques. This has turned the area into one of the best locations for performing intercomparisons between different standard candles. By adding our PNLF measurements to those of the SBF and GCLF techniques, we can test for the systematic errors in all three techniques and quantitatively assess the accuracy of each method.

In §2 of this paper, we describe our observations of three galaxies in the Coma I cloud, NGC 4494, NGC 4565, and the small E1 elliptical NGC 4278, and present measurements of 255 newly identified planetary nebula (PN) candidates, including two "overluminous" objects. In §3 and 4, we present our PNLF distances to these galaxies and find support for the SBF and GCLF contention that the group has a substantial line-of-sight thickness, and thus is not as well-mixed as originally believed. We conclude by discussing the possible origins of the overluminous sources, and considering a modified PNLF law that takes into account the existence of objects brighter than the nominal PNLF cutoff.

2. OBSERVATIONS

Our observations were obtained in the spring of 1992 and 1995 with the prime focus of the Kitt Peak 4-m telescope and the T2KB 2048 × 2048 Tektronix CCD, which has a pixel scale of $0''.47$. The field of view of the CCD, $16'.3 \times 16'.3$, encompassed all of NGC 4278 and 4494, and included all but the outermost regions of NGC 4565. Table 1 summarizes the two runs involved. All our narrow-band images were 1 hour exposures; our intermediate band off-line images were 9 minute integrations. While NGC 4278 was observed under excellent conditions, the observations of NGC 4494 and NGC 4565 were complicated by periods of poor seeing and occasional thin cirrus.

Consequently, the usable data on these latter two galaxies consisted of the best 6 (of 8) exposures for NGC 4494 and the best 3 (of 6) frames for NGC 4565. Those frames used in the final coadded image are noted in Table 1.

Our PN survey technique was as described in previous papers of the series (see, for example, Jacoby *et al.* 1989). Each galaxy was imaged in both a narrow-band filter transmitting ~ 30 Å around the [O III] λ5007 emission line (shifted to match the redshift of the galaxy), and through a wider off-band filter transmitting ~ 300 Å centered near 5275 Å. PN candidates were identified both by blinking the on-band/off-band image pairs, and also by selecting positive residuals on "difference" images that were formed by subtracting our scaled continuum images from their on-band counterparts. Although our grand sum images were all built using software that rejects radiation events (the IRAF IMCOMBINE task), each PN candidate was also visually examined to be certain that it exhibited a normal stellar point spread function (PSF) rather than the atypical pattern associated with "cosmic rays."

For the elliptical galaxies NGC 4278 and NGC 4494, we assumed that contamination of our PN sample by HII regions is unlikely (but see §5). For the Sb galaxy NGC 4565, however, HII regions are abundantly evident. To minimize the confusion caused by these objects, we applied the following safeguards. First, we rejected any spatially resolved emission source, since PN at ~ 10 Mpc are always stellar. Second, we obtained a 1 hour Hα image of NGC 4565 to derive an approximate ratio $R = I(\lambda5007)/I(\mathrm{H}\alpha)$ for each object; bright PN strongly tend to $R \sim 3$ whereas H II regions normally have $R \leq 1$. Third, we avoided objects within $20''$ (~ 1 kpc) of the plane of this nearly edge-on (inclination $\sim 86°$; de Vaucouleurs 1958) galaxy. With these filters applied, we expect that few, if any, interloper HII regions remain in our PN sample. In all, we identified 39 PN candidates in NGC 4278, 183 in NGC 4494, and 35 in NGC 4565.

Equatorial coordinates for all the PN and several reference stars were derived with the *Hubble Space Telescope* (HST) Guide Star catalog to define the coordinate system of each galaxy field. Within each field, the coordinate systems have uncertainties of $\sim 0''.5$.

Photometry of the PN candidates was performed relative to field stars on each frame with the DAOPHOT point-spread-function fitting routines (Stetson 1987) within IRAF. For NGC 4494 and 4565, the magnitudes of the field stars were determined by comparing their large aperture magnitudes to those of four Stone (1977) spectrophotometric standard stars (BD+25 3941, BD+8 2015, Feige 34, and Kopff 27) taken on the night of UT 6 April 1992. Although this night appeared photometric, the 0.04 mag dispersion in the zero-point solution derived from these standards is somewhat higher than the 0.02 mag generally seen, and suggests that thin clouds may have been present during the observations. NGC 4278's field stars were calibrated in a similar manner with the Stone (1977) and Oke (1974) spectrophotometric standards G191B2B, Feige 34, and BD+33 2642. This latter calibration was performed on two different nights; the difference between the two nights was less than 0.02 mag.

For the final step in our reductions, we computed the standard magnitudes for the PNe

using the photometric procedures for emission-line objects described by Jacoby, Quigley, & Africano (1987). The filter transmission curves, corrected for the f/2.7 beam of the telescope and the temperature of the filter at the telescope, are illustrated in Figure 1. The assumed galactic systemic velocities were taken from the Third Reference Catalog of Bright Galaxies (de Vaucouleurs *et al.* 1991; RC3), while the envelope velocity dispersions for NGC 4278 and 4494 were estimated from Davies & Birkinshaw (1988) and Jedrzejewski & Schechter (1989). The halo PN of NGC 4565 were assumed to have a velocity dispersion of ~ 100 km s^{-1}.

Tables 2-4 list the PN candidates identified in the three galaxies, their epoch 2000 coordinates, and their λ5007 magnitudes as defined by Ciardullo *et al.* (1989a),

$$m_{5007} = -2.5 \log F_{5007} - 13.74. \quad (1)$$

The mean errors in the photometric measurements, as reported by the PSF-fitting algorithms of DAOPHOT, are listed in Table 5 as a function of m_{5007}. Table 6 gives the positions of astrometric reference stars.

3. DISTANCES

3.1. Defining the Statistical Samples

Plots of the raw PNLFs are shown in Figure 2. The fact that each PNLF begins near a bright limit of $m_{5007} \sim 25.6$ indicates that all three galaxies are crudely at the same distance. The turndown at magnitudes fainter than $m_{5007} \gtrsim 26.7$ is due to incompleteness, and confirms that the observing conditions for NGC 4278 were substantially better than those for NGC 4494 or 4565.

In order to form a statistical sample of PN in each galaxy, we began by considering the detectability of a planetary nebula versus galactic radius. The signal-to-noise of a PN measurement depends both on the magnitude of the object and on the brightness of the background galaxy. Hence the threshold for PN detection decreases as one searches closer in towards the galaxy nucleus. To avoid variations in our detection limits, we formed our statistical samples using only those objects projected in regions where the surface brightness of the underlying galaxy is less than that of the background sky. Theoretical and empirical tests have shown that when samples are defined in this way, the limiting magnitude for completeness is very nearly the place where the raw PNLF begins to drop (Ciardullo *et al.* 1987; Ciardullo *et al.* 1989b; Hui *et al.* 1993). Moreover, small (~ 0.1 mag) errors in the definition of this limit have little or no effect on the derived distances. Thus, for NGC 4278, our statistical sample included only those PN brighter than $m_{5007} = 27.1$ that are projected outside the galaxy's isophote at $1\farcm5$ (semi-major axis); for NGC 4494, the sample consisted of PN with $m_{5007} < 27.0$ and isophotal radii $R_{iso} > 1\farcm0$. For the spiral galaxy NGC 4565, our sample of objects consisted of PN projected more than $20''$ from the galactic plane and with $m_{5007} < 26.5$. This information is summarized in Table 7. The isophotal radius or z distance of each planetary nebulae is included in Tables 2–4. Those PN that are part

of the statistical samples are marked with an "S."

Before deriving distances, one additional remark should be made concerning the PN candidates of NGC 4278. An inspection of Figure 2 shows that, while the PNLFs of NGC 4494 and 4565 exhibit a sharp cutoff at the bright end of the luminosity function, NGC 4278's luminosity function also has a conspicuous overluminous tail. The brightest of NGC 4278's [O III] λ5007 sources is nearly 1 mag brighter than the apparent PNLF cutoff; the second brightest object is ~ 0.5 mag brighter than the break. Remarkably, both sources are, in reality, intracluster in origin: PN candidate #1 is projected more than $10r_e$ from the galaxy's nucleus, while candidate #2 is almost $15r_e$ from the galactic center, where r_e is the effective radius of the galaxy.

Strictly speaking, the two "overluminous" objects listed in Table 4 are not planetary nebula candidates. A deep Hα image taken during the course of a nova survey of NGC 4278 (Shafter, Ciardullo, & Pritchet 1996) reveals that the brightest [O III] λ5007 source is even brighter in Hα. This suggests that the candidate is either a supernova remnant or an H II region, and should be excluded from the analysis. Similarly, although PN candidate #2 is invisible in Hα and thus has the excitation of a planetary nebula, a careful inspection of its image shows that it is marginally resolved with an intrinsic FWHM of $\sim 0\farcs6$. Hence it, too, should be omitted from our sample. Both objects are included in our PN table for purposes of completeness: had the galaxy been further away, or not been surveyed for novae, both would have been classified as "overluminous PN candidates." We will return to these objects in §5.

3.2. Maximum Likelihood Solutions

The PNLF distances to NGC 4278, 4494, and 4565 and their formal uncertainties were calculated by convolving the empirical function (Ciardullo *et al.* 1989a)

$$N(M) \propto e^{0.307M} \left[1 - e^{3(M^* - M)}\right] \tag{2}$$

with the photometric errors of Table 5 and fitting the resultant curve to the observed PNLFs via the method of maximum likelihood (Ciardullo *et al.* 1989a). As in previous studies, we adopted $M^* = -4.48$, based on a distance to M31 of 710 kpc (Welch *et al.* 1986), a foreground reddening of $E(B-V) = 0.11$ (McClure & Racine 1969), and a Seaton (1979) reddening curve. With more recent values for M31's distance (770 kpc; Freedman & Madore 1990) and reddening ($E(B-V) = 0.08$; Burstein & Heiles 1984), the distances reported here would increase by $\sim 3\%$. All our Coma I distances have assumed the foreground extinction values (see Table 7) of Burstein & Heiles (1984).

The maximum likelihood fits to the observed statistical PNLFs are summarized in Table 7 and shown in Figure 3. Figure 4 displays the uncertainty of each solution via probability contours. Note that the ordinate of Figure 4 is $\alpha_{2.5}$, the number of PN within 2.5 mag of M^* normalized to galactic bolometric luminosity. The luminosity normalization of NGC 4278 is based on the surface

photometry of Peletier *et al.* (1990); the normalizations for NGC 4494 and 4565 are derived from B and V CCD photometry performed with the Kitt Peak 0.9-m telescope. Bolometric corrections for NGC 4278 and 4494 were estimated by combining the ultraviolet observations of Burstein *et al.* (1988) with the infrared and optical colors given by Johnson (1966), Frogel *et al.* (1978), and RC3. The bolometric correction for NGC 4565's halo is an estimate based on the observed $B-V$ color. Note that although the amount of luminosity sampled in NGC 4278 and 4494 is similar, the latter galaxy has a factor of 10 more planetaries in the top ~ 0.9 mag of its PNLF. This is a result of fundamental differences between the two stellar populations: NGC 4278 has a significant excess of emission in the *IUE* bandpass ($m_{1550}-V = 2.88$), while the UV upturn in NGC 4494 is very mild ($m_{1550}-V = 3.77$; Burstein *et al.* 1988). The anti-correlation between UV excess and $\alpha_{2.5}$ seen in the two galaxies adds support to the suggestion by Ciardullo, Jacoby, & Harris (1991) and Ferguson & Davidsen (1993) that the ultraviolet flux emitted by old stellar populations comes from stars whose asymptotic branch evolution has been prematurely aborted (Greggio & Renzini 1990; Dorman, Rood, & O'Connell 1993). Similar correlations between galaxy properties (B-V, luminosity) and PN production rates were first noted by Peimbert (1990). These topics will be discussed in detail in a separate paper (Ciardullo, Jacoby, & Feldmeier 1996).

3.3. Uncertainties

The uncertainties implied by the contours of Figure 4 are only those internal to the fitting procedure. To compute the total error budget, these uncertainties must be combined with those associated with photometric zero points, the filter response curves, and the Galactic foreground extinctions. (The latter come from Burstein & Heiles 1984.) In addition, two systemic errors, which affect all PNLF measurements the same way, arise from the uncertain definition of the empirical PNLF, and, of course, the distance to the calibration galaxy, M31. These errors are summarized in Table 8.

4. DEPTH OF THE COMA I GROUP

The primary motivation of this study was to assess the reliability of the PNLF method across Hubble types. Our PNLF distances to the 3 members of the group, NGC 4278, 4494, and 4565, are $10.2^{+0.5}_{-0.8}$, $12.8^{+0.5}_{-0.5}$, and $10.5^{+0.5}_{-0.7}$ Mpc. (Here, we have omitted the possible systematic contribution to the errors.) A comparison of these distances suggests that there is indeed a small, but significant, difference between the distance to the large elliptical NGC 4494 and that of the other two galaxies. Either NGC 4278 and 4565 are ~ 2 Mpc in front of NGC 4494, or the PNLF distance method is affected by stellar population or sample size.

To test the plausibility of these two alternatives, we plot in Figure 5, the positions of the three galaxies based on distances derived from the PNLF, GCLF, and SBF techniques. These are

summarized in Table 10. All three methods agree that the distance to NGC 4565 is $\sim$ 10 Mpc, but, more importantly, each method finds that NGC 4494 is in the background. According to the SBF method, NGC 4494 and 4565 are separated by 4.6 ± 2.1 Mpc (Simard & Pritchet 1994), the GCLF technique gives a separation of 4.4 ± 3.3 Mpc (Fleming *et al.* 1995), and the PNLF measurements imply a separation of 2.3 ± 0.8 Mpc. Since all three methods are strikingly different in detail, it is extremely unlikely that the error estimates of the techniques are correlated. This being the case, and if the error bars are accurate, there is less than a 0.1% chance that the two galaxies are members of the same $\sim$ 1 Mpc size cluster.

Simard & Pritchet (1994) and Fleming *et al.* (1995) note the fact that the galaxies of Coma I fall near the "triple-value ambiguity" of Virgocentric infall models (e.g., Tonry & Davis 1981; Tully & Shaya 1984). Here, the Hubble flow in the direction of Coma I, which is 13° from Virgo, is complicated by Virgo's gravitational attraction. According to the infall model, galaxies having similar radial velocities (1259 km/s for NGC 4494 and 1171 km/s for NGC 4565, corrected to the centroid of the Local Group) can be located at distances of $\sim$ 10–11, $\sim$ 14–15, or $\sim$ 21–24 Mpc, depending on the choices for the Virgo distance and Hubble Constant. The PNLF distance measurements to NGC 4565 and 4494 are consistent with those models.

Moreover, the fact that the three methods considered here all produce similar results enhances the arguments of Jacoby *et al.* (1992), Ciardullo, Jacoby, & Tonry (1993), and Jacoby (1995) that most distance indicators yield completely consistent results. Recent PNLF and HST Cepheid distances for M101, for example, yield nearly identical values. Feldmeier, Ciardullo, & Jacoby (1996) obtained 7.7 ± 0.5 Mpc using the PNLF while Kelson *et al.* (1994) found 7.5 ± 0.7 Mpc with Cepheids. Previous direct PNLF–Cepheid comparisons in M81, NGC 5253, and NGC 300 also yielded excellent agreement (see Soffner *et al.* 1995). Similarly, Tanvir *et al.* (1995) derived an HST Cepheid distance to M96 of 11.6 ± 0.8 Mpc. This agrees well with the PNLF distance of 10.4 ± 1.3 Mpc to NGC 3377, NGC 3384, and NGC 3379 (values from Ciardullo, Jacoby, & Ford 1989b, but corrected to the modern M31 distance and reddening), the companion early-type galaxies to M96 in the Leo group.

5. OVERLUMINOUS [O III] OBJECTS AND THE PNLF

As mentioned above, the PNLF of NGC 4278 is somewhat confused by the presence of "overluminous" objects – that is, objects with an [O III] λ5007 magnitude substantially brighter than m^*. (Here, we define "substantially" as more than 0.2 mag more luminous than m^*; normal PN may occasionally be recorded as being slightly overluminous due to random photometric error.) We were able to exclude these objects on the basis of their Hα emission and angular extent. However, this information is not always available; had NGC 4278 been at the distance of Virgo, PN #2 would have been included in the complete sample. Similarly, without an Hα image, PN #1 would also have been included. Moreover, the existence of this tail would have called into question the nature of PN #3, which is $\sim$ 0.2 mag brighter than the next brightest object.

Table 9 lists all the overluminous [O III] λ5007 sources discovered to date, along with their parent galaxies and properties. To be included in the list, an object must have an [O III] λ5007 magnitude more than 0.2 mag brighter that m^*, and be indistinguishable from a PN in 1.″2 seeing at the distance of Virgo.

5.1. What Are the Overluminous Sources?

In order to deal with the problem of overluminous [O III] λ5007 in a PN sample, we must first have some idea as to their origin. There are many possibilities.

H II regions: In some sense, the simplest explanation for the overluminous [O III] λ5007 sources is compact H II regions. At distances of $\gtrsim$ 10 Mpc, typical ground-based cameras with 1″ seeing cannot resolve objects smaller than $\sim$ 30 pc; thus, smaller objects can appear stellar and be identified as planetary nebulae. In 0.″8 seeing, Ciardullo *et al.* (1991) resolved one overluminous object in NGC 1023. Also, PN #2 in NGC 4278 is marginally resolved in 1.″3 seeing with an implied linear size of $\sim$ 30 pc. These objects cannot be PN, since bright planetaries are never larger than $\sim$ 1 pc. They can, however, be compact H II regions, which have diameters down to $\sim$ 10 pc (Kennicutt 1984). While we generally do not expect to see HII regions in elliptical galaxies, some early-type systems, and NGC 4278 in particular, often host pockets of ionized gas. Figure 6 illustrates that NGC 4278 is an interesting example: after subtracting the continuum image from the [O III] image, an extensive pattern similar to a barred spiral galaxy is revealed.

While we cannot rule out H II regions as being responsible for the overluminous sources, there are several problems with this interpretation. First, although many of the host galaxies in Table 9 are known to contain gas and/or dust, evidence for star formation in them is generally absent. We thus are faced with the question of why the host galaxies are creating compact H II regions, but not larger, more typical ones. Second, although the sample of overluminous PN is small, the tendency is for these objects to be located at large galactic radii. Under most scenarios, star formation should occur closer to the galactic centers, where the density is higher and the gas is more easily shocked. Finally, the excitation of at least some of these bright sources is much higher than that of a typical H II region. The ratio of Hα to [O III] in NGC 4486's overluminous PN is $\lesssim$ 0.5, and PN candidate #2 in NGC 4278 was undetectable in a 1 hour Hα image taken with the Kitt Peak 4-m telescope.

Supernova remnants: Type Ia supernovae occur in early-type galaxies, though at a lower rate than in late-type galaxies (van den Bergh & McClure 1994; van den Bergh & Tammann 1991). In fact, of the 6 galaxies listed in Table 9, three (NGC 4374, 4382, and 4486) have hosted supernovae in this century alone. However, none of these supernovae was detected in [O III] λ5007 (Jacoby, Ciardullo & Ford 1990), nor were 1980N and 1981D detected in the planetary nebula survey of NGC 1316 (McMillan, Ciardullo, & Jacoby 1993). This is consistent with the hypothesis presented in Jacoby, Ciardullo, & Ford (1990) that supernovae will be difficult to detect when the interstellar

medium in a galaxy is sparse: without a confining medium, the supernova shell will quickly expand to an undetectable low density, low surface brightness state. It may be significant, however, that NGC 4278 is embedded in a disk of atomic hydrogen that extends $\sim 9r_e$ into the galaxy's halo (Raimond *et al.* 1981; Burstein, Krumm, & Salpeter 1987; Lees 1992). Thus, the overluminous objects detected in this galaxy may indeed be the confined remnants of recent supernovae. This is especially true of NGC 4278 PN #1, which is bright in Hα as well as [O III]. Future imaging in [S II] would help discriminate supernova remnants from HII regions.

Wolf-Rayet nebulae: The strong winds and UV emission from Wolf-Rayet stars can interact with their surrounding interstellar medium to create ring nebulae that are similar to planetary nebulae (Chu 1993). Even in the Milky Way, the two can be extremely difficult to distinguish: the nebula M1-67 (Minkowski 1946), for example, was classified as a planetary by Bertola (1964), but has since been reclassified as a Wolf-Rayet nebula by Cohen & Barlow (1975), put back in the planetary nebula category by van der Hucht *et al.* (1985), and returned yet again to Wolf-Rayet status by Esteban *et al.* (1991) and Crawford & Barlow (1991). Unlike the central stars of PN, Wolf-Rayet stars can have very high masses (10 – 50 $M_\odot$; Massey 1981) and luminosities; hence, their nebulae can have the extreme luminosity of an overluminous [O III] source. However, since the Wolf-Rayet phenomenon is short-lived, any association of these objects with the overluminous PN implies the presence of a substantial population of young, very massive stars in otherwise normal elliptical galaxies.

Supersoft x-ray nebulae: Di Stefano, Paerels, & Rappaport (1995) have modeled the luminosity function expected for nebulae surrounding supersoft x-ray sources. These sources, which may be low mass x-ray binaries (Cowley *et al.* 1990) or white dwarfs undergoing steady nuclear burning due to accretion (Rappaport, Di Stefano, & Smith 1994), can extend the PNLF by nearly 1 mag, *if* they happen to be surrounded by cold interstellar gas. Unfortunately, the only known example of the class, CAL 83, (Pakull, Ilovaisky, & Chevalier 1985; Remillard, Rappaport, & Macri 1995) is 10 times fainter than M^*, and quite extended ($\sim$ 25 pc). Support for the association of overluminous PN with supersoft x-ray sources, does come, however, from N67, a bright, normal PN in the Small Magellanic Cloud, that is coincident with the Einstein ultrasoft x-ray source 1E0056.8−7154 (Wang 1991; Brown *et al.* 1994).

PN from massive progenitors: By modeling the [O III] λ5007 luminosities expected from ensembles of PN, Jacoby (1989) found that for a PN to become $\sim$ 1 mag brighter than M^*, its central star must be more massive than 0.72 $M_\odot$. From the initial-to-final mass relations of Kwok (1983) and Weidemann (1987), this implies a progenitor mass of $\gtrsim$ 4 $M_\odot$ (late B on the main sequence). Since stars of this high mass are extremely short-lived, the probability of catching one near maximum luminosity is very low (see Figure 1 of Jacoby 1989). Thus, in order to see PN descended from young stars, a substantial population I component is needed. This is unlikely for a normal elliptical galaxy, although a population of intermediate mass progenitors with ages of $\sim$ 3 Gyrs may explain the existence of objects $\lesssim$ 0.2 mag brighter than M^*.

Coalesced binaries: Iben & Tutukov (1989) have pointed out that $\sim$ 15% of all planetary nebulae

should be formed during the interaction of close binary stars. For these objects, the expected mass distribution of central stars is distorted. Some PN will end up with anomalously low mass cores, as a result of aborted core evolution during the common envelope phase. Alternatively, if the spiral-down of a common envelope binary is extreme, the two components may merge and create a high mass core. Yungelson, Tutukov, & Livio (1993) have estimated that this latter scenario will typically produce central stars in the range of 0.75–0.80 $M_\odot$ — exactly that required for the overluminous objects. There is strong evidence that at least $\sim$ 15% of Galactic planetaries do indeed descend from a common envelope stage of evolution (Bond 1989; Bond & Livio 1990), and at least two planetary nebula central stars (EGB 5 and PHL 932) have been proposed as being the products of coalescence (Méndez *et al.* 1988a,b). However, the problem of stellar evolution inside common envelopes is complex and poorly constrained; no unambiguous case for a coalesced binary exists, and no Milky Way counterpart of the overluminous objects is known.

Chance superposition of PN: Figure 7 of Ciardullo, Jacoby, & Harris (1991) illustrates that the superposition of two fainter PN can lead to the identification of an "overluminous" source. In that example, two bright PN in the S0 galaxy NGC 1023 combined to create an object that was apparently overluminous by $\sim$ 0.3 mag. It was only when the seeing became 0.″8 that the two sources could be resolved. Statistical experiments show that these coincidences should occur often enough to enhance the PNLF in the luminosity range 0.1–0.2 mag beyond M^* (Jacoby, Ciardullo, & Ford 1990). We intentionally exclude this luminosity range from our definition of overluminous objects partly for this reason. However, superpositions cannot explain sources more luminous than $\sim$ 0.4 mag beyond M^*, nor are they reasonable candidates for the distant halo objects. In addition, spectroscopy of PN #1 in NGC 4486 shows only a single emission line at 5007 Å. If superposition is at work here, the unlikely condition must be that both objects have the same radial velocity.

Background quasars: Quasars with $z \sim 3.1$ will have their Lyα emission redshifted into the 5007 Å filter bandpass. To be identified as a PN candidate, though, the continuum emission must be suppressed by $\sim$ 3 mag below the emission-line flux. While unlikely, this possibility can only be excluded for PN #1 in NGC 4486, where spectroscopy demonstrates that the emission line is, indeed, [O III] λ5007.

5.2. Revising the Empirical PNLF

As stated above, the existence of overluminous [O III] λ5007 sources in a sample of planetary nebulae causes a problem for the maximum likelihood method. Because the empirical law of equation 2 makes no provision for objects brighter than M^*, the presence of even one such source can distort the results from the fit. If a PN candidate is sufficiently overluminous, its exclusion from the sample can be justified on the basis of the resulting fit (i.e., the most-likely PNLF solution is excluded by a χ^2 or Kolmogorov-Smirnov statistic). However, an object that is $\sim$ 0.2 mag overluminous cannot be excluded in this way, and, depending on the circumstances, its

inclusion in the sample may change the derived distance to a galaxy by $\sim 10\%$.

There is no statistically correct way to handle overluminous sources. If the luminosity function of these objects were known, *and* if the function were the same in every galaxy, then the empirical PNLF could be modified easily to include their contribution. Unfortunately, the rarity and uncertain origin of the phenomenon prevents us from knowing either of these things. In fact, in contrast to the luminosity function of normal planetary nebulae, there is good reason to believe that the luminosity function of overluminous objects is *not* the same in every galaxy. NGC 4278, which is a small elliptical, has two PN candidates that might qualify as overluminous; NGC 4494, which has 7 times more normal PN than 4278, has none. Similarly, the giant ellipticals of Fornax, NGC 1399, 1316, and 1404, contain no overluminous PN, while NGC 4374 and 4406 in Virgo have two each. Whether this variation is due to differences in stellar population or interstellar medium, the fact remains that the number of overluminous sources in a galaxy does not scale with the population of normal PN, nor does it scale with any obvious galaxy property (e.g., luminosity or color).

The problems presented by the existence of overluminous objects can be illustrated by modifying the empirical PNLF in order to take into account the occasional appearance of interlopers. Assuming the luminosity function of contaminating objects is flat, we can express the observed luminosity function of all [O III] λ5007 sources as

$$\begin{aligned} N(M) &\propto K + e^{0.307M}[1 - e^{3(M^*-M)}], \quad \text{if } M > M^* \\ N(M) &\propto K, \qquad\qquad\qquad\quad \text{if } (M^* - 1) < M < M^* \end{aligned} \tag{3}$$

where K represents the non-zero likelihood of finding a contaminating source in any given magnitude interval. Given that between 1 and 2% of all extragalactic PN brighter than $M_{5007} = -4.0$ are overluminous, $K \sim 0.005$.

If this formulation were applied to the PN (and overluminous objects) of NGC 4278, the best fitting distance to the galaxy would be almost ~ 0.3 mag smaller than the nominal value of $(m - M)_0 = 30.04$. Moreover, the error on this distance would be a full ~ 0.4 mag, or three times larger than the present error estimate. This change in the character of the solution comes from the normalization of K: in order to fit a PNLF, in which $\sim 30\%$ of the bright PN are overluminous, K has to be an order of magnitude larger. Without this large value of K, the PNLF cutoff is forced to brighter magnitudes, and the estimated uncertainty is increased by the large number of (equally bad) solutions. It is possible, of course, to artificially increase K in order to compensate for the relatively large number of background contaminants, (and this does recover the original distance modulus), but solutions with this added variable are ill-defined. This is especially true with the small sample sizes frequently encountered in planetary nebula surveys.

The best way to correct for overluminous objects, of course, is to exclude them ahead of time, using their Hα emission or spatial extent. As Table 9 illustrates, one-third of the overluminous

objects discovered to date are resolvable in good seeing, and, at least one other is bright in Hα. Thus, every attempt should be made to throw out possible contaminants *a priori*. If this cannot be done, then the safest approach is to compute the PNLF distances with and without the suspect interlopers, and to include the two different results when computing the total uncertainty in the PNLF distance.

6. CONCLUSIONS

Our primary motivation for studying the Coma I group of galaxies was to test for a Hubble type dependence in the PNLF technique via internal (PNLF vs. PNLF) and external (PNLF vs. SBF vs. GCLF) comparisons. Somewhat surprisingly, our data, and that of the SBF and GCLF methods, suggest that the galaxies of the group are not all at a common distance. This has compromised the value of an internal test. However, external comparisons of PNLF distances against distances derived from the SBF and GCLF methods are still valuable. We find that:

1. The PNLF, GCLF, and SBF methods place the E1 galaxy NGC 4494 2 – 4 Mpc more distant than the edge-on spiral NGC 4565. The separation is smallest for the PNLF method, so if one wants to attribute the difference in distance to a Hubble type dependence, the bias is smallest for the PNLF. We are not aware of any other technique that places these two galaxies closer together than $\sim$ 2 Mpc. Indeed, we are not aware of any other method that provides a measurement to both systems. There are few techniques that can be applied across such a wide range in Hubble types.

2. The PNLF distances to the E1 galaxy NGC 4278 and the Sb galaxy 4565 are essentially identical. If we had chosen to test the PNLF method with only these two galaxies, we would have concluded that there is no Hubble type dependence. That was the result we found in the NGC 1023 group. Thus, it is evident that larger samples of galaxies are required to detect the presence of systematic biases in PNLF distances (or those from any other technque) at the low levels (5-10%) we are probing.

3. The PNLF, GCLF, and SBF techniques continue to yield consistent results at the 5-10% level. Agreement for all three methods to the edge-on Sb galaxy, NGC 4565, is superb, having a sample dispersion of only $\pm$4%. This is rather remarkable, considering that all three methods are more commonly applied to early-type systems. For NGC 4494, the dispersion is 7%, still excellent by the standards of the field.

In addition, we find evidence that the luminosity function for overluminous [O III] sources is highly variable from galaxy to galaxy. This is not too surprising, considering that we identify 8 plausible origins for these very rare (11) sources. We note that nearly half the sources classified as overluminous can be rejected as PN either on the basis of their size (resolved objects are larger than $\gtrsim$ 25 pc, and consequently, are too large to be PN), or their line ratios (bright PN must be high excitation objects). Thus, in cases of ambiguity, high resolution imaging or imaging at other

wavelengths can be used to exclude many interlopers.

We have attempted to refine our measurement algorithms to accommodate the low probability of overluminous sources contaminating the PNLF. Unfortunately, the lack of a known or constant luminosity function for these sources renders the prescription of limited value. Overluminous [O III] sources are rare, however, and usually they fall sufficiently off the nominal PNLF to be rejected as outliers during the fitting process. Consequently, they have little or no impact on PNLF distances.

RC was supported in part by NASA grant NAGW-3159 and NSF grant AST92-57833. WEH acknowledges financial support from the Natural Sciences and Engineering Research Council of Canada. We wish to thank Karen Kwitter for helpful discussions regarding Wolf-Rayet nebulae, and Sidney van den Bergh for helpful suggestions to improve the presentation of this paper.

Table 1. Observing Log

Galaxy	Date	Filter	Seeing, arcsec	Sky	In Coadded Image
NGC 4278	4 Apr 95	5016/31	1.4	clear	Yes
	4 Apr 95	5016/31	1.4	clear	Yes
	4 Apr 95	5016/31	1.4	clear	Yes
	5 Apr 95	5016/31	1.2	thin cirrus	Yes
	4 Apr 95	5312/267	1.3	clear	Yes
	4 Apr 95	5312/267	1.2	clear	Yes
	4 Apr 95	5312/267	1.2	clear	Yes
	5 Apr 95	5312/267	1.4	thin cirrus	Yes
NGC 4494	6 Apr 92	5025/32	2.2	clear	No
	6 Apr 92	5025/32	1.4	clear	Yes
	6 Apr 92	5025/32	2.1	clear	No
	7 Apr 92	5025/32	1.6	cirrus	Yes
	7 Apr 92	5025/32	1.3	cirrus	Yes
	7 Apr 92	5025/32	1.2	cirrus	Yes
	7 Apr 92	5025/32	1.0	cirrus	Yes
	7 Apr 92	5025/32	1.1	cirrus	Yes
	6 Apr 92	5290/285	2.0	clear	No
	6 Apr 92	5290/285	1.9	clear	No
	6 Apr 92	5290/285	2.0	clear	No
	7 Apr 92	5290/285	1.1	cirrus	Yes
	7 Apr 92	5290/285	1.2	cirrus	Yes
	7 Apr 92	5290/285	1.2	cirrus	Yes
	7 Apr 92	5290/285	1.2	cirrus	Yes
NGC 4565	4 Apr 92	5025/32	1.4	cirrus	Yes
	4 Apr 92	5025/32	1.4	cirrus	Yes
	4 Apr 92	5025/32	1.7	cirrus	No
	5 Apr 92	5025/32	1.4	clear	Yes
	5 Apr 92	5025/32	1.6	cirrus	No
	6 Apr 92	5025/32	2.2	clear	No
	7 Apr 92	6619/62	1.9	cirrus	Yes

Table 1—Continued

Galaxy	Date	Filter	Seeing, arcsec	Sky	In Coadded Image
	4 Apr 92	5312/267	2.1	cirrus	No
	4 Apr 92	5312/267	2.1	cirrus	No
	4 Apr 92	5312/267	2.0	cirrus	No
	4 Apr 92	5312/267	2.0	cirrus	No
	6 Apr 92	5290/285	1.8	clear	No
	6 Apr 92	5290/285	1.9	clear	No
	6 Apr 92	5290/285	2.1	clear	No
	6 Apr 92	5290/285	2.1	clear	No
	6 Apr 92	5290/285	1.6	clear	Yes
	6 Apr 92	5290/285	1.6	clear	Yes
	6 Apr 92	5290/285	1.3	clear	Yes
	6 Apr 92	5290/285	1.6	clear	Yes

TABLE 2
NGC 4278 PLANETARY NEBULAE

ID	α(2000)	δ(2000)	$R_{iso}(')$	m_{5007}	Notes	ID	α(2000)	δ(2000)	$R_{iso}(')$	m_{5007}	Notes
1	12 20 28.94	29 15 49.4	5.7	25.03	Hα	21	12 19 55.18	29 19 38.9	4.5	26.78	S
2	12 20 23.36	29 11 13.5	8.1	25.45	Resolved	22	12 19 49.49	29 16 22.1	4.1	26.83	S
3	12 20 10.95	29 18 15.5	1.7	25.74	S	23	12 20 04.20	29 15 40.2	1.3	26.84	
4	12 20 01.08	29 18 52.0	2.7	25.96	S	24	12 20 04.69	29 15 30.2	1.4	26.91	
5	12 20 22.02	29 15 34.3	4.1	26.01	S	25	12 20 07.38	29 23 49.7	7.7	26.94	S
6	12 20 21.92	29 15 51.9	4.0	26.15	S	26	12 19 50.95	29 15 18.4	3.9	26.94	S
7	12 20 10.36	29 16 52.6	0.9	26.25		27	12 19 59.88	29 15 43.7	1.9	26.97	S
8	12 19 36.61	29 14 59.3	7.3	26.26	S	28	12 20 21.54	29 16 07.4	3.8	26.98	S
9	12 20 26.56	29 19 20.5	5.1	26.35	S	29	12 19 56.60	29 13 53.0	3.7	27.02	S
10	12 20 23.50	29 16 13.2	4.2	26.35	S	30	12 20 02.37	29 15 15.5	1.8	27.05	S
11	12 19 54.71	29 14 20.4	3.6	26.36	S	31	12 19 45.79	29 11 40.9	6.9	27.15	
12	12 20 01.06	29 15 52.2	1.6	26.54	S	32	12 19 59.10	29 18 30.3	2.7	27.17	
13	12 20 18.40	29 17 08.5	2.8	26.59	S	33	12 20 13.53	29 23 08.5	6.8	27.18	
14	12 20 05.01	29 13 42.8	3.3	26.61	S	34	12 20 02.64	29 20 10.4	3.9	27.18	
15	12 20 16.47	29 14 40.3	3.5	26.65	S	35	12 19 34.50	29 16 25.1	7.9	27.19	
16	12 20 03.45	29 17 20.2	1.0	26.66		36	12 20 01.14	29 15 21.7	1.9	27.22	
17	12 20 12.72	29 16 06.6	1.7	26.67	S	37	12 19 59.72	29 15 44.5	1.9	27.30	
18	12 20 07.16	29 13 36.4	3.5	26.68	S	38	12 19 50.24	29 17 56.1	4.3	27.39	
19	12 20 10.46	29 17 48.5	1.3	26.76		39	12 19 56.86	29 14 40.1	3.0	27.67	
20	12 20 09.76	29 18 33.8	1.9	26.78	S						

TABLE 3
NGC 4494 PLANETARY NEBULAE

ID	α(2000)	δ(2000)	$R_{iso}(')$	m_{5007}	Notes
1	12 31 23.19	25 46 53.0	0.5	25.68	
2	12 31 25.68	25 46 09.5	0.5	25.90	
3	12 31 21.78	25 47 02.9	0.9	25.99	
4	12 31 21.45	25 46 07.2	0.8	26.01	
5	12 31 22.84	25 45 41.3	0.9	26.06	
6	12 31 25.97	25 46 09.5	0.6	26.13	
7	12 31 20.23	25 47 31.4	1.4	26.15	S
8	12 31 27.03	25 46 02.3	0.9	26.16	
9	12 31 24.08	25 47 41.5	1.2	26.17	S
10	12 31 29.87	25 45 55.5	1.5	26.17	S
11	12 31 28.97	25 45 33.2	1.5	26.17	S
12	12 31 15.07	25 47 19.7	2.5	26.19	S
13	12 31 11.92	25 46 38.3	3.2	26.19	S
14	12 31 16.16	25 46 35.9	2.1	26.21	S
15	12 31 18.29	25 46 29.4	1.5	26.30	S
16	12 31 23.08	25 45 55.6	0.6	26.30	
17	12 31 23.04	25 45 51.6	0.7	26.32	
18	12 31 23.37	25 47 14.9	0.8	26.32	
19	12 31 22.94	25 47 11.6	0.8	26.33	
20	12 31 21.65	25 47 09.4	0.9	26.34	
21	12 31 27.49	25 47 13.5	1.2	26.35	S
22	12 31 22.96	25 45 44.9	0.8	26.36	
23	12 31 24.65	25 46 58.6	0.5	26.36	
24	12 31 30.07	25 47 13.1	1.7	26.37	S
25	12 31 27.50	25 47 01.1	1.0	26.37	S
26	12 31 14.33	25 46 22.7	2.5	26.39	S
27	12 31 21.90	25 46 57.3	0.8	26.40	
28	12 31 23.47	25 47 33.0	1.1	26.41	S
29	12 31 15.07	25 45 33.8	2.5	26.41	S
30	12 31 20.40	25 46 53.4	1.1	26.42	S
31	12 31 27.00	25 45 53.8	0.9	26.42	
32	12 31 19.56	25 47 12.2	1.4	26.43	S
33	12 31 24.55	25 47 54.8	1.5	26.43	S
34	12 31 22.62	25 45 47.7	0.8	26.43	
35	12 31 18.56	25 48 10.5	2.2	26.44	S
36	12 31 24.99	25 45 10.8	1.3	26.44	S
37	12 31 24.06	25 47 06.8	0.6	26.44	
38	12 31 22.52	25 46 00.1	0.6	26.45	
39	12 31 23.52	25 45 27.8	1.0	26.45	S
40	12 31 22.50	25 46 46.1	0.5	26.46	
41	12 31 22.56	25 47 48.1	1.4	26.46	S
42	12 31 21.55	25 46 39.9	0.7	26.47	
43	12 31 30.10	25 46 00.2	1.6	26.48	S
44	12 31 23.24	25 45 47.7	0.7	26.48	
45	12 31 18.48	25 46 57.0	1.5	26.48	S
46	12 31 23.33	25 45 08.9	1.3	26.48	S
47	12 31 19.55	25 46 29.3	1.2	26.49	S
48	12 31 27.87	25 44 34.8	2.1	26.50	S
49	12 31 30.36	25 47 03.7	1.7	26.50	S
50	12 31 17.07	25 45 57.0	1.9	26.50	S
51	12 31 20.99	25 46 35.5	0.8	26.51	
52	12 31 30.12	25 46 23.9	1.5	26.51	S
53	12 31 27.59	25 46 30.3	0.9	26.51	
54	12 31 27.27	25 47 08.9	1.1	26.53	S
55	12 31 22.74	25 46 56.5	0.6	26.53	
56	12 31 19.47	25 47 00.5	1.3	26.53	S
57	12 31 28.73	25 44 33.9	2.2	26.54	S
58	12 31 28.12	25 45 18.4	1.5	26.55	S
59	12 31 13.80	25 44 50.4	3.2	26.55	S
60	12 31 18.20	25 46 53.0	1.6	26.55	S
61	12 31 25.78	25 45 42.2	0.9	26.56	
62	12 31 20.18	25 47 29.0	1.4	26.56	S
63	12 31 18.05	25 44 13.4	2.8	26.57	S
64	12 31 29.98	25 45 53.0	1.6	26.57	S
65	12 31 22.18	25 45 48.7	0.8	26.57	
66	12 31 16.54	25 44 13.8	3.0	26.59	S
67	12 31 26.56	25 43 36.3	2.9	26.61	S
68	12 31 22.88	25 45 58.3	0.6	26.61	
69	12 31 28.55	25 46 59.1	1.3	26.61	S
70	12 31 21.04	25 47 19.4	1.2	26.62	S
71	12 31 23.73	25 45 24.3	1.1	26.62	S
72	12 31 32.23	25 45 52.3	2.2	26.63	S
73	12 31 23.09	25 45 27.4	1.0	26.63	S
74	12 31 35.48	25 46 14.2	2.9	26.63	S
75	12 31 20.46	25 46 23.5	1.0	26.64	
76	12 31 22.57	25 46 50.7	0.6	26.64	
77	12 31 26.14	25 47 43.0	1.4	26.64	S
78	12 31 28.09	25 46 48.6	1.1	26.64	S
79	12 31 37.03	25 43 26.1	4.5	26.64	S
80	12 31 24.15	25 47 45.9	1.3	26.66	S
81	12 31 28.39	25 43 52.7	2.8	26.66	S
82	12 31 28.69	25 46 19.3	1.2	26.67	S
83	12 31 29.48	25 47 07.3	1.5	26.67	S
84	12 31 18.12	25 46 02.5	1.6	26.68	S
85	12 31 25.70	25 47 12.1	0.9	26.69	
86	12 31 15.07	25 47 06.1	2.4	26.69	S
87	12 31 21.97	25 46 48.2	0.7	26.69	
88	12 31 25.00	25 47 26.1	1.0	26.70	S
89	12 31 25.00	25 47 02.2	0.6	26.70	
90	12 31 18.85	25 43 32.0	3.3	26.71	S
91	12 31 19.49	25 45 42.5	1.4	26.72	S
92	12 31 29.42	25 46 56.1	1.5	26.72	S
93	12 31 14.60	25 45 12.7	2.8	26.72	S
94	12 31 29.08	25 46 32.0	1.3	26.73	S
95	12 31 22.31	25 46 42.3	0.6	26.74	
96	12 31 10.84	25 45 29.7	3.6	26.74	S
97	12 31 19.56	25 46 14.2	1.2	26.75	S
98	12 31 29.15	25 46 33.3	1.3	26.75	S
99	12 31 15.30	25 46 58.9	2.3	26.75	S
100	12 31 19.27	25 42 50.1	3.9	26.76	S
101	12 31 23.49	25 48 13.9	1.8	26.76	S
102	12 31 27.78	25 46 44.1	1.0	26.78	S
103	12 31 30.83	25 46 01.8	1.7	26.78	S
104	12 31 33.27	25 46 53.4	2.4	26.78	S
105	12 31 28.66	25 45 05.0	1.8	26.79	S
106	12 31 21.70	25 45 39.2	1.0	26.80	S
107	12 31 27.48	25 45 12.7	1.5	26.80	S
108	12 31 26.64	25 45 36.4	1.1	26.81	S
109	12 31 12.30	25 48 20.5	3.6	26.83	S
110	12 31 13.88	25 44 15.4	3.5	26.83	S

TABLE 3 — *Continued*

ID	α(2000)	δ(2000)	$R_{iso}(')$	m_{5007}	Notes	ID	α(2000)	δ(2000)	$R_{iso}(')$	m_{5007}	Notes
111	12 31 20.08	25 48 29.8	2.3	26.83	S	148	12 31 19.52	25 47 05.3	1.3	27.04	
112	12 31 29.80	25 45 42.1	1.6	26.83	S	149	12 31 25.54	25 47 20.3	0.9	27.04	
113	12 31 18.26	25 44 40.5	2.4	26.84	S	150	12 31 32.64	25 46 07.5	2.2	27.05	
114	12 31 22.87	25 45 14.9	1.3	26.85	S	151	12 31 23.28	25 47 25.9	1.0	27.06	
115	12 31 37.04	25 49 00.4	4.2	26.86	S	152	12 31 37.37	25 47 29.5	3.6	27.06	
116	12 31 23.24	25 44 45.6	1.7	26.88	S	153	12 31 26.92	25 45 27.0	1.2	27.08	
117	12 31 35.19	25 46 36.5	2.9	26.89	S	154	12 31 23.78	25 47 36.2	1.1	27.10	
118	12 31 31.29	25 47 33.6	2.2	26.91	S	155	12 31 21.00	25 47 50.9	1.6	27.10	
119	12 31 16.26	25 44 49.0	2.6	26.92	S	156	12 31 20.72	25 47 25.1	1.3	27.11	
120	12 31 20.66	25 46 16.9	0.9	26.92		157	12 31 30.95	25 44 01.0	3.0	27.12	
121	12 31 24.95	25 47 23.3	0.9	26.93		158	12 31 27.62	25 44 51.0	1.8	27.12	
122	12 31 19.69	25 44 15.0	2.5	26.93	S	159	12 31 35.32	25 47 53.4	3.3	27.12	
123	12 31 30.90	25 44 04.1	2.9	26.93	S	160	12 31 32.59	25 45 50.4	2.2	27.14	
124	12 31 31.03	25 47 47.5	2.2	26.94	S	161	12 31 26.36	25 45 35.9	1.0	27.15	
125	12 31 20.85	25 45 39.7	1.2	26.95	S	162	12 31 34.62	25 44 54.2	3.1	27.17	
126	12 31 30.88	25 45 46.3	1.8	26.95	S	163	12 31 18.53	25 44 10.6	2.8	27.17	
127	12 31 22.19	25 45 32.7	1.1	26.95	S	164	12 31 25.23	25 47 21.9	0.9	27.18	
128	12 31 20.80	25 46 20.5	0.9	26.96		165	12 31 18.01	25 47 02.3	1.6	27.18	
129	12 31 27.52	25 46 48.3	0.9	26.96		166	12 31 18.69	25 45 25.4	1.8	27.19	
130	12 31 24.52	25 47 38.4	1.2	26.97	S	167	12 31 24.94	25 44 46.1	1.7	27.20	
131	12 31 17.30	25 44 05.4	3.0	26.97	S	168	12 31 18.09	25 46 11.1	1.6	27.20	
132	12 31 21.72	25 45 28.7	1.2	26.98	S	169	12 31 28.48	25 46 19.3	1.1	27.21	
133	12 31 24.08	25 47 09.8	0.7	26.98		170	12 31 14.12	25 43 39.9	3.9	27.21	
134	12 31 18.92	25 45 09.8	1.9	26.98	S	171	12 31 18.17	25 47 03.1	1.6	27.22	
135	12 31 30.13	25 44 52.2	2.2	26.98	S	172	12 31 34.55	25 47 46.5	3.0	27.23	
136	12 31 33.25	25 45 16.1	2.6	26.98	S	173	12 31 32.34	25 43 30.9	3.6	27.23	
137	12 31 23.65	25 48 08.6	1.7	26.98	S	174	12 31 36.70	25 46 32.9	3.3	27.24	
138	12 31 16.05	25 45 15.7	2.4	26.98	S	175	12 31 27.27	25 47 32.4	1.4	27.27	
139	12 31 24.04	25 48 19.1	1.9	26.98	S	176	12 31 19.25	25 45 33.6	1.6	27.27	
140	12 31 21.34	25 47 54.7	1.6	27.00	S	177	12 31 35.74	25 47 56.3	3.4	27.28	
141	12 31 23.98	25 47 11.3	0.7	27.02		178	12 31 25.89	25 43 35.3	2.9	27.34	
142	12 31 36.48	25 45 19.5	3.4	27.02		179	12 31 36.72	25 45 31.1	3.4	27.36	
143	12 31 19.04	25 45 35.1	1.6	27.02		180	12 31 22.00	25 47 17.4	1.0	27.38	
144	12 31 19.20	25 45 28.8	1.6	27.02		181	12 31 32.52	25 45 46.0	2.2	27.59	
145	12 31 24.16	25 44 52.4	1.6	27.03		182	12 31 18.82	25 45 24.2	1.8	27.65	
146	12 31 33.45	25 49 14.5	3.7	27.03		183	12 31 19.26	25 45 40.0	1.5	27.69	
147	12 31 27.28	25 48 23.3	2.1	27.04							

TABLE 4

NGC 4565 PLANETARY NEBULAE

ID	α(2000)	δ(2000)	$z(")$	m_{5007}	Notes	ID	α(2000)	δ(2000)	$z(")$	m_{5007}	Notes
1	12 36 16.52	25 59 32.4	28	25.76	S	19	12 36 16.77	25 58 57.8	50	26.47	S
2	12 36 26.38	25 57 28.5	20	25.86	S	20	12 36 14.85	26 01 20.0	32	26.49	S
3	12 36 21.62	25 58 23.5	27	25.91	S	21	12 36 15.21	26 01 11.4	29	26.58	
4	12 36 20.04	25 58 22.9	43	25.91	S	22	12 36 29.59	25 56 35.3	26	26.58	
5	12 36 21.81	25 58 14.1	32	26.00	S	23	12 36 25.97	25 58 44.8	30	26.59	
6	12 36 28.64	25 58 30.0	45	26.09	S	24	12 36 24.00	25 57 50.7	27	26.63	
7	12 36 29.56	25 57 49.4	25	26.16	S	25	12 36 14.53	25 59 55.8	31	26.71	
8	12 36 13.49	25 59 59.8	37	26.17	S	26	12 36 25.05	25 59 37.1	58	26.71	
9	12 36 09.00	26 03 04.0	49	26.19	S	27	12 36 41.03	25 55 18.1	29	26.72	
10	12 36 15.75	25 59 21.9	43	26.20	S	28	12 36 05.39	26 02 14.7	20	26.76	
11	12 36 36.33	25 56 01.6	15	26.26		29	12 36 30.41	25 56 28.0	23	26.82	
12	12 36 12.88	26 00 25.6	25	26.28	S	30	12 36 30.61	25 56 31.7	19	26.99	
13	12 36 31.60	25 57 20.4	25	26.29	S	31	12 36 18.55	25 57 52.8	78	27.02	
14	12 36 27.62	25 56 12.1	61	26.30	S	32	12 36 10.14	26 01 05.7	23	27.19	
15	12 36 27.41	25 56 20.2	58	26.31	S	33	12 36 12.07	26 00 17.1	39	27.22	
16	12 36 35.26	25 57 14.4	56	26.32	S	34	12 36 07.03	25 58 24.5	166	27.41	
17	12 36 13.52	26 02 06.6	52	26.42	S	35	12 36 08.86	25 58 50.0	131	27.77	
18	12 36 04.65	26 02 22.7	22	26.44	S						

Table 5. PN Photometric Error versus Magnitude

Magnitude	NGC 4278	NGC 4494	NGC 4565
25.00	0.03	...	...
25.25	...	...	...
25.50	0.05	...	...
25.75	0.06	...	0.07
26.00	0.07	...	0.07
26.25	0.08	0.10	0.08
26.50	0.09	0.11	0.10
26.75	0.10	0.12	0.12
27.00	0.12	0.14	0.16
27.25	0.15	0.16	0.19
27.50	0.18	0.20	0.22

TABLE 6

ASTROMETRIC REFERENCE STARS

Galaxy	ID	α(2000)	δ(2000)
NGC 4278	a	12 19 53.64	29 13 18.2
	b	12 20 11.13	29 13 54.3
	c	12 20 23.53	29 15 55.4
	d	12 19 48.10	29 15 09.0
	e	12 19 59.68	29 21 55.0
	f	12 20 11.97	29 12 39.5
	g	12 20 27.16	29 19 08.5
	h	12 20 10.06	29 22 37.0
	i	12 19 35.59	29 22 34.3
	j	12 20 38.61	29 20 05.0
	k	12 20 44.08	29 20 01.6
NGC 4494	a	12 31 17.01	25 46 19.2
	b	12 31 16.78	25 47 12.0
	c	12 31 10.94	25 43 12.3
	d	12 31 05.68	25 50 43.0
	e	12 31 03.39	25 50 42.9
	f	12 31 37.12	25 40 10.1
	g	12 31 43.20	25 39 20.2
	h	12 31 54.53	25 50 56.2
	i	12 31 55.23	25 38 34.4
	j	12 31 09.31	25 48 45.5
	k	12 31 15.94	25 47 01.9
	l	12 31 11.74	25 43 54.4
NGC 4565	a	12 36 44.32	25 55 49.4
	b	12 36 01.53	26 01 13.3
	c	12 35 59.49	26 00 44.6
	d	12 36 16.82	26 03 54.3
	e	12 36 24.76	26 05 39.4
	f	12 36 32.68	26 06 14.0
	g	12 35 56.55	26 03 07.9
	h	12 36 18.87	25 52 07.3
	i	12 36 13.25	25 51 45.6
	j	12 36 04.62	25 54 25.3
	k	12 36 47.93	25 58 27.5
	l	12 35 50.98	25 57 16.3
	m	12 35 54.09	25 57 03.9
	n	12 35 55.57	25 58 07.9
	o	12 36 08.61	25 58 27.1
	p	12 36 12.22	25 59 52.0
	q	12 36 03.48	26 04 16.5
	r	12 36 37.10	25 57 43.2
	s	12 36 38.64	26 04 45.2
	t	12 36 10.09	25 56 57.4
	u	12 36 08.46	25 56 21.9
	v	12 36 46.40	26 00 34.4
	w	12 36 44.49	26 05 17.6

Table 7. Summary For Coma I Galaxies

Parameter	NGC 4278	NGC 4494	NGC 4565
Galaxy Type (RSA)	E1	E1	Sb
BT (RC3)	11.09	10.71	10.42
Systemic Vel (km/s)	649	1324	1227
A_B (B&H)	0.10	0.06	0.04
Separation from NGC 4565	4.9°	1.1°	....
V(sampled)	11.2	11.0	10.8
PN completeness limit	27.1	27.0	26.5
Location of completeness	R(iso) > 90"	R(iso) > 60"	z > 20"
Number of PN found	39	183	35
Number of PN in sample	23	101	17
Best fitting $(m-M)_0$	$30.04^{+0.08}_{-0.16}$	$30.54^{+0.04}_{-0.05}$	$30.12^{+0.07}_{-0.13}$
$\alpha_{2.5}$	$10.5^{+2.4}_{-2.0}$	$49.3^{+5.5}_{-4.8}$	$11.7^{+3.5}_{-2.6}$

Table 8. Summary of Magnitude Uncertainties

Source	NGC 4278	NGC 4494	NGC 4565
Maximum likelihood fit	$^{+0.08}_{-0.16}$	$^{+0.04}_{-0.05}$	$^{+0.07}_{-0.13}$
Photometric zero point	0.02	0.04	0.04
Filter response	0.04	0.04	0.04
Foreground extinction	0.05	0.05	0.05
Total random error	$^{+0.10}_{-0.17}$	$^{+0.09}_{-0.09}$	$^{+0.10}_{-0.15}$
PNLF definition	0.05	0.05	0.05
M31 distance	0.10	0.10	0.10
Total Error (random + systematic)	$^{+0.15}_{-0.21}$	$^{+0.14}_{-0.14}$	$^{+0.15}_{-0.19}$

Table 9. Summary of λ5007 Overluminous Sources

Galaxy	ID	$M^* - M_{5007}$	Nr PN	Comments
NGC 1023	...	0.5	110	Resolved in 0.″8 seeing; gas rich galaxy
NGC 4278	1	0.6	39	Stellar in 1.″3 seeing; $\frac{I(\mathrm{H}\alpha)}{I(\lambda 5007)} \gtrsim 1$; gas rich galaxy
	2	0.2		Resolved in 1.″3 seeing
NGC 4382	1	1.1	102	Stellar in 1.″0 seeing; blue S0 galaxy
NGC 4406	1	1.0	141	Stellar in 1.″1 seeing
	2	0.3		Resolved in 1.″1 seeing
	3	0.2		Stellar in 1.″1 seeing
NGC 4374	1	0.3	102	Stellar in 1.″1 seeing
	2	0.2		Stellar in 1.″1 seeing
	3	0.2		Resolved in 1.″1 seeing
NGC 4486	1	0.8	340	Stellar in 0.″7 seeing; $\frac{I(\mathrm{H}\alpha)}{I(\lambda 5007)} \lesssim 0.5$; single narrow line

Table 10. Comparison of Distances to Coma I Galaxies

Galaxy	GCLF[a]	SBF[b]	PNLF[c]
NGC 4278	...	...	$10.2^{+0.7}_{-1.0}$
NGC 4494	14.5 ± 2.7	15.0 ± 1.9	$12.8^{+0.9}_{-0.9}$
NGC 4565	10.0 ± 1.5	10.4 ± 0.5	$10.5^{+0.8}_{-1.0}$

[a]Fleming *et al.* 1995

[b]Simard & Pritchet 1994

[c]This paper assumed the M31 distance and reddening of 710 kpc and E(B-V)=0.11, respectively; distances increase by 3% when adopting more recent parameters.

REFERENCES

Bertola, F. 1964 PASP, 76, 241

Bond, H.E. 1989, in IAU Symposium 131, Planetary Nebulae, edited by S. Torres-Peimbert (Kluwer, Dordrecht), p. 251

Bond, H.E., & Livio, M. 1990, ApJ, 355, 568

Brown. T., Cordova, F., Ciardullo, R., Thompson, R., & Bond, H. 1994, ApJ, 422, 118

Burstein, D., Bertola, F., Buson, L.M., Faber, S.M., Lauer, T.R. 1988, ApJ, 328, 440

Burstein, D., & Heiles, C. 1984, ApJS, 54, 33

Burstein, D., Krumm, N., & Salpeter, E.E. 1987, AJ, 94, 883

Chu, Y.-H. 1993, in IAU Symposium 155, Planetary Nebulae, edited by R. Weinberger & A. Acker (Kluwer, Dordrecht), p. 139

Ciardullo, R., Ford, H.C., Neill, J.D., Jacoby, G.H., & Shafter, A.W. 1987, ApJ, 318, 520

Feldmeier, J., Ciardullo, R., & Jacoby, G.H. 1995, ApJ, in preparation

Ciardullo, R., Jacoby, G.H., & Feldmeier, J. 1996, ApJ, in preparation

Ciardullo, R., Jacoby, G.H, Ford, H.C., & Neill, J.D., 1989a, ApJ, 339, 53

Ciardullo, R., Jacoby, G.H., & Ford, H.C. 1989b, ApJ, 344, 715

Ciardullo, R., Jacoby, G.H., & Harris, W.E., 1991, ApJ, 383, 487

Ciardullo, R., Jacoby, G.H., & Tonry, J.L. 1993, ApJ, 419, 479

Cohen, M. & Barlow, M. J. 1975, Astrophys. Lett., 16, 165

Cowley, A.P., Schmidtke, P.C., Crampton, D., & Hutchings, J.B. 1990, ApJ, 350, 288

Crawford, I.A., & Barlow, M.J. 1991, A&A, 249, 518

Davies, R.L., & Birkinshaw, M. 1988, ApJS, 68, 409

de Vaucouleurs, G. 1958, ApJ, 127, 487

de Vaucouleurs, G. 1975, in Stars and Stellar Systems IX, Galaxies and the Universe, edited by A. Sandage, M. Sandage, & J. Kristian (University of Chicago Press, Chicago), p. 557

de Vaucouleurs, G., de Vaucouleurs, A., Corwin, H.G. Jr., Buta, R.J., Paturel, G., & Fouqué, P. 1991, Third Reference Catalog of Bright Galaxies (Springer-Verlag, New York) (RC3)

Di Stefano, R., Paerels, F., & Rappaport, S. 1995, ApJ, 450, 705

Dorman, B., Rood, R.T., & O'Connell, R.W. 1993, ApJ, 419, 596

Esteban, C., Vílchez, J.M., Smith, L.J., & Manchado, A. 1991, A&A, 244, 205

Ferguson, H.C., & Davidsen, A.F. 1993, ApJ, 408, 92

Fleming, D.B., Harris, W.E., Pritchet, C.J., & Hanes, D.A. 1995, AJ, 109, 1044

Freedman, W.L., & Madore, B.F. 1990, ApJ, 365, 186

Frogel, J.A., Persson, S.E., Aaronson, M., & Matthews, K. 1978, ApJ, 220, 75

Greggio, L., & Renzini, A. 1990, ApJ, 364, 35

Hamuy, M., Phillips, M.M., Maza, J., Suntzeff, N.B., Schommer, R.A., & Avilés, R. 1995, AJ, 109, 1

Hui, X., Ford, H.C., Ciardullo, R., & Jacoby, G.H. 1993, ApJ, 414, 463

Iben, I., & Tutukov, A.V. 1989, in IAU Symposium 131, Planetary Nebulae, edited by S. Torres-Peimbert (Kluwer, Dordrecht), p. 505

Jacoby, G. H. 1989, ApJ, 339, 39

Jacoby, G.H. 1995, in Science With the VLT, edited by J. Walsh & I.J. Danziger (Springer, Heidelberg), p. 267

Jacoby, G.H., Ciardullo, R., & Ford, H.C. 1990, ApJ, 356, 332

Jacoby, G.H., Ciardullo, R., Ford, H.C., & Booth, J. 1989, ApJ, 344, 704

Jacoby, G.H., Quigley, R.J., & Africano, J.L. 1987, PASP, 99, 672

Jacoby, G.H., Branch, D., Ciardullo, R., Davies, R.L., Harris, W.E., Pierce, M.J., Pritchet, C.J., Tonry, J.L., & Welch, D.L. 1992, PASP, 104, 599

Jedrzejewski, R., & Schechter, P.L. 1989, AJ, 98, 147

Johnson, H.L. 1966, ApJ, 143, 187

Kelson, D.D., Illingworth, G.D., Freedman, W.L, Hill, R., Graham, J.A., Saha, A., Madore, B.F., Mould, J.R., Hughes, S.M.G., Stetson, P.B., Kennicutt, R.C., Ferrarese, L., Ford, H.C., Hoessel, J.G., & Huchra, J. 1994, BAAS, 26, 1352

Kennicutt, R.C. 1984, ApJ, 287, 116

Kwok, S. 1983, in IAU Symposium 103, Planetary Nebulae, edited by D.R. Flower (Reidel, Dordrecht), p. 293

Lees, J.F. 1992, Ph.D. Thesis, Princeton University.

Massey, P. 1981, ApJ, 246, 153

McClure, R.D., & Racine, R. 1969, AJ, 74, 1000

McMillan, R., Ciardullo, R., & Jacoby, G.H. 1993, ApJ, 416, 62

Méndez, R.H., Groth, H.G., Husfeld, D., Kudritzki, R.P., & Herrero, A. 1988b, A&A, 197, L25

Méndez, R.H., Kudritzki, R.P., Herrero, A., Husfeld, D., & Groth, H.G. 1988a, A&A, 190, 113

Minkowski, R., 1946, PASP, 58, 305

Oke, J.B. 1974, ApJS27, 21

Pakull, M.W., Ilovaisky, S., & Chevalier, C. 1985, Space Sci. Rev., 40, 229

Peimbert, M. 1990, Rev Mex A&Ap, 20, 119

Peletier, R.F., Davies, R.L., Illingworth, G.D., Davis, L.E., & Cawson, M. 1990, AJ, 100, 1091

Raimond, E., Faber, S.M., Gallagher, J.S. III, & Knapp, G.R. 1981, ApJ, 246, 708

Rappaport, S., Di Stefano, R., & Smith, J.D. 1994, ApJ, 426, 692

Remillard, R., Rappaport, R., & Macri, L. 1995, ApJ, 439, 646

Seaton, M.J. 1979, MNRAS, 187, 73p

Shafter, A.W., Ciardullo, R., & Pritchet, C.J. 1996, ApJ, in preparation

Simard, L. & Pritchet, C.J. 1994, AJ, 107, 503

Soffner, T., Méndez, R.H., Jacoby, G.H., Ciardullo, R., Roth, M.M., & Kudritzki, R.P. 1995, A&A, in press

Stetson, P.B. 1987, PASP, 99, 191

Stone, R.P.S. 1977, ApJ, 218, 767

Tanvir, N.R., Shanks, T., Ferguson, H.C., and Robinson, D.R.T. 1995, Nature, 377, 27

Tonry, J.L., & Davis, M. 1981, ApJ, 246, 680

Tully, R.B., & Shaya, E.J. 1984, ApJ, 281, 31.

van den Bergh, S., & McClure, R.D. 1994, ApJ, 425, 205

van den Bergh, S., & Tammann, G.A. 1991, ARA&A, 29, 363

van der Hucht, K.A., Jurriens, T.A., Olnon, F.M., Thé, P.S., Wesselius, P.R., & Williams, P.M. 1985, A&A, 145, L13

Wang, Q. 1991, MNRAS252, 47p

Weidemann, V. 1987, A&A, 188, 74

Welch, D.L., McAlary, C.W., McLaren, R.A., & Madore, B.F. 1986, ApJ, 305, 583

Yungelson, L.R., Tutukov, A.V., & Livio, M. 1993, ApJ, 418, 794

Fig. 1.— The transmission curves for the two on-band filters used in this survey. The dashed line illustrates the filter used for NGC 4278; the solid line defines the filter employed for NGC 4494 and 4565. Both curves are for observations taken in the converging f/2.7 beam of the Kitt Peak 4-m prime focus, and account for the wavelength shift caused by the ambient temperature (10° C for NGC 4278, 8° C for NGC 4494 and 4565). The wavelengths of [O III] λ5007 at the systemic velocities of the galaxies are marked.

Fig. 2.— The raw PNLFs of NGC 4278, 4494, and 4565. Magnitudes are defined as in Ciardullo *et al.* (1989a) and equation 1. Although the PNLFs are generally similar in form, it is apparent that the PNLF for NGC 4565 becomes incomplete at a significantly brighter limit than for NGC 4278 or 4494. Also apparent are the 2 overluminous objects of NGC 4278: although neither is a true PN, they are included here for completeness.

Fig. 3.— The PNLFs for NGC 4278, 4494, and 4565 as defined by those PN in the homogeneously complete sample (solid points). Open circles indicate those objects fainter than the completeness limit. Objects 1 and 2 in Table 2 were omitted from this plot because they are not PN. The solid lines represent the empirical PNLF of equation 1 convolved with the mean photometric error vs. magnitude relation and translated to the most likely distance modulus for each galaxy.

Fig. 4.— Maximum likelihood contours for NGC 4278, 4494, and 4565 derived from fitting the empirical PNLF (convolved with the photometric error function) to complete samples of PN in each galaxy. The abscissa is the true distance modulus; the ordinate is the number of PN within 2.5 mag of the bright end magnitude cutoff, normalized to the amount of bolometric luminosity surveyed. The probability contours are drawn at 0.5σ intervals. Due to the difficulty in estimating the luminosity and bolometric correction applicable to NGC 4565's halo, the vertical scale for this galaxy is somewhat uncertain.

Fig. 5.— A graphical representation of the distances in Table 10, but the PNLF distances have been increased by 3% to place them on the same M31 zero point system as the other methods. It is clear that NGC 4278 and 4565 have similar distances as measured by their PNLFs, but all three methods place NGC 4494 further away. Given the quoted errors in the methods, it is very likely that NGC 4565 and 4494 are not members of the same $\sim$ 1 Mpc size cluster.

Fig. 6.— The central $11' \times 11'$ of the [O III] difference image of the elliptical galaxy NGC 4278. North is displayed up and east to the left. Although classified as an E1 galaxy, NGC 4278 has a small amount of ionized gas distributed in a barred spiral pattern. Filaments of the gas extend to the edge of the figure, well beyond the usual optical image; one filament apparently passes very close to the small E0 galaxy NGC 4283 which appears as a strong negative (white) residual to the north-east of NGC 4278. There is no evidence for a physical association, otherwise, and NGC 4283 has a velocity $\sim$ 500 km/s higher than NGC 4278. Raimond *et al.* (1981) suggested that a central bar might be present to explain the regular disk-like kinematics of an HI cloud that envelopes NGC 4278. They also noted a central hole in the HI emission, which we suggest may be due to the

gas being ionized, and they hypothesized that the source of the gas could be from a cannibalized gas-rich dwarf. This [OIII] image supports those ideas. The diagonal streak running from due north to the southeast is a satellite trail.

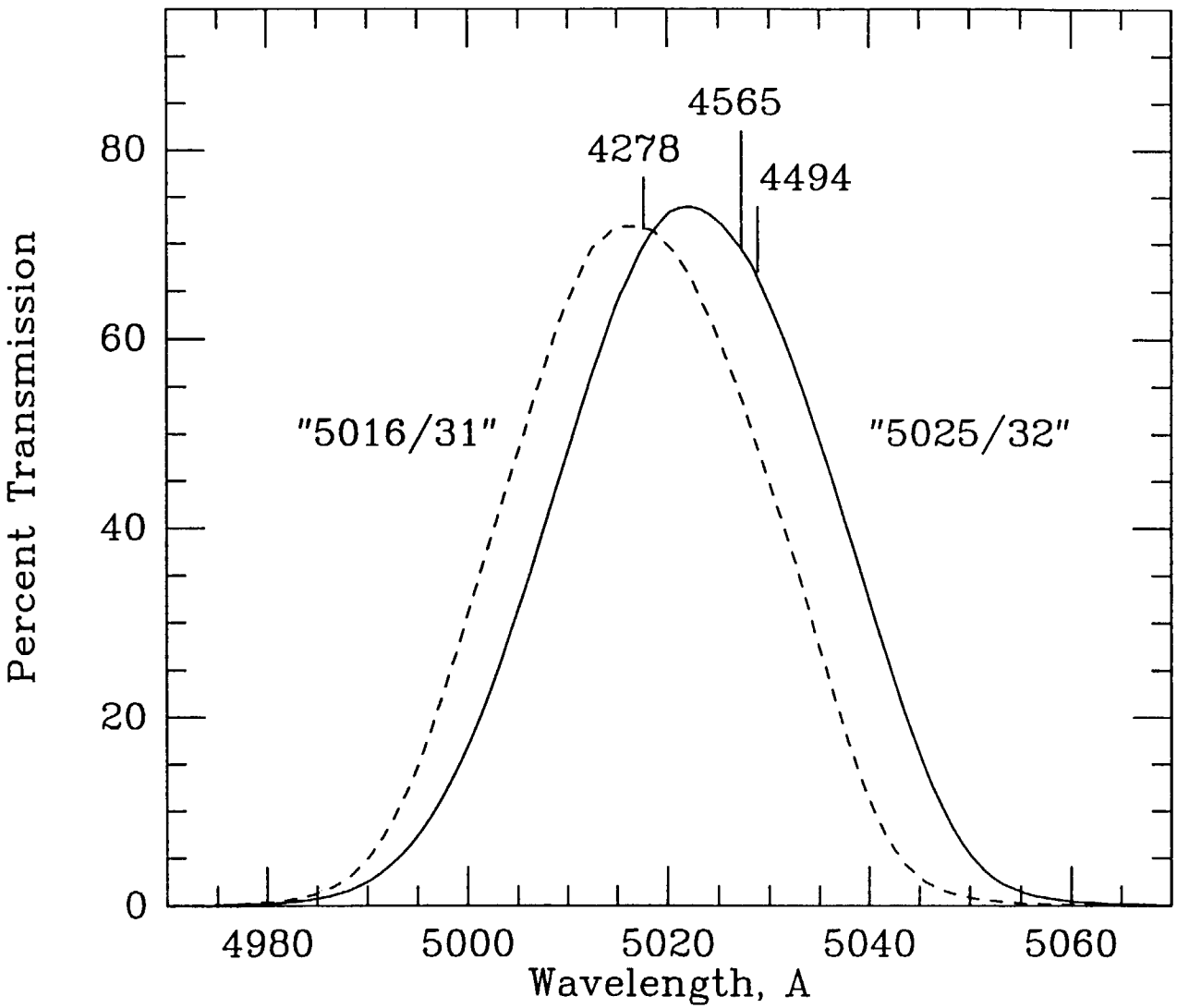

Fig. 1 - Jacoby et al

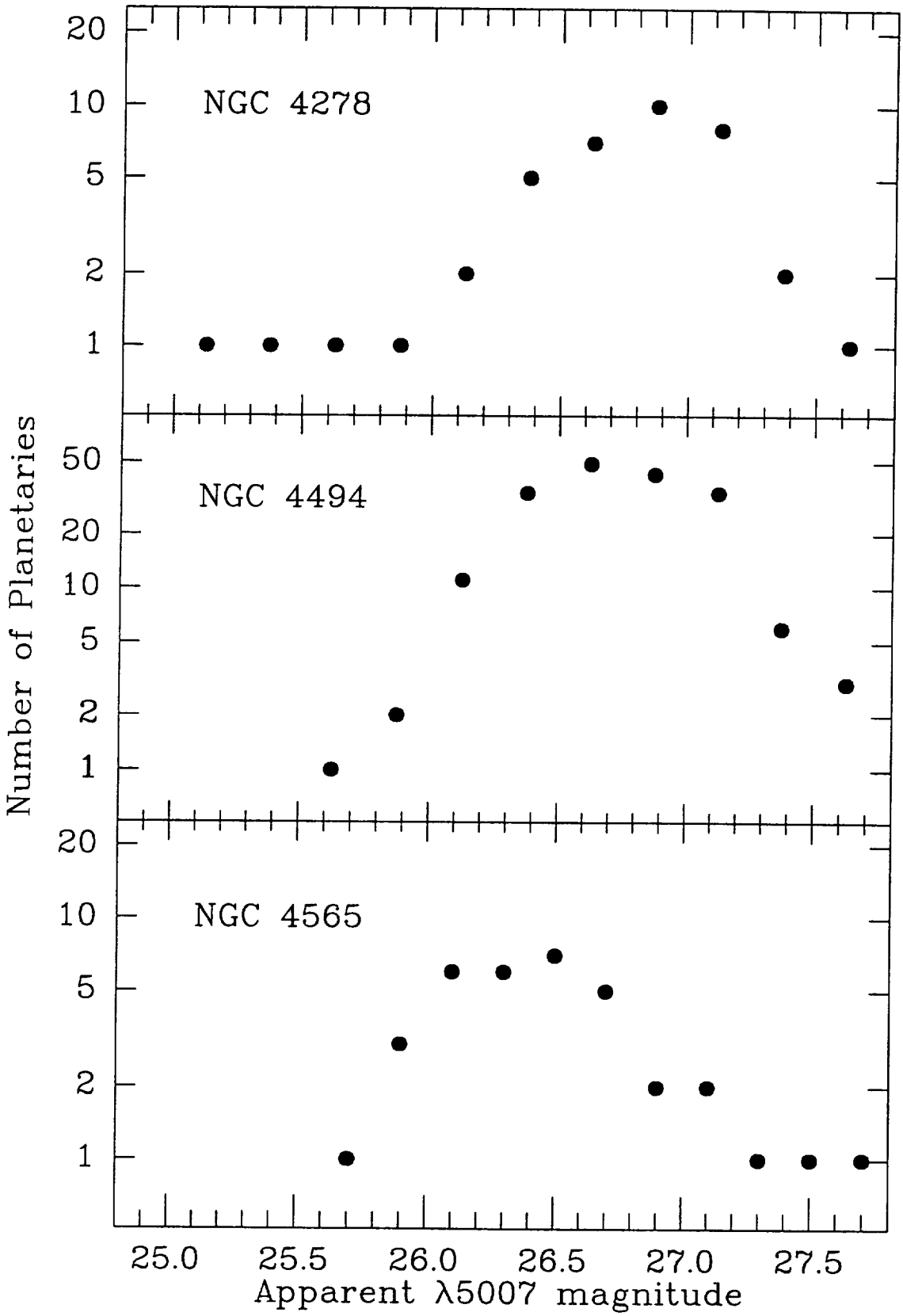

Fig. 2 - Jacoby et al

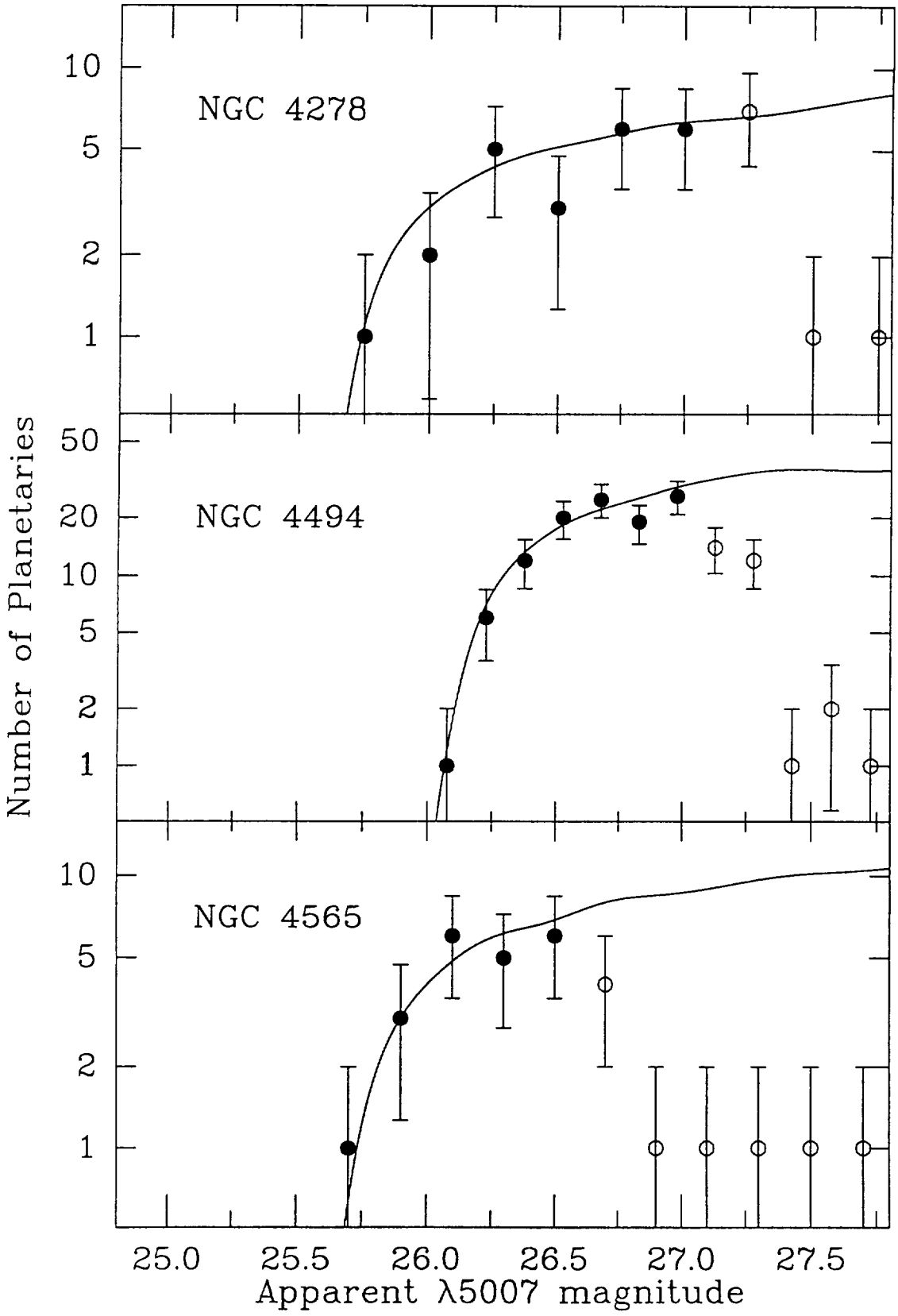

Fig. 3 - Jacoby et al

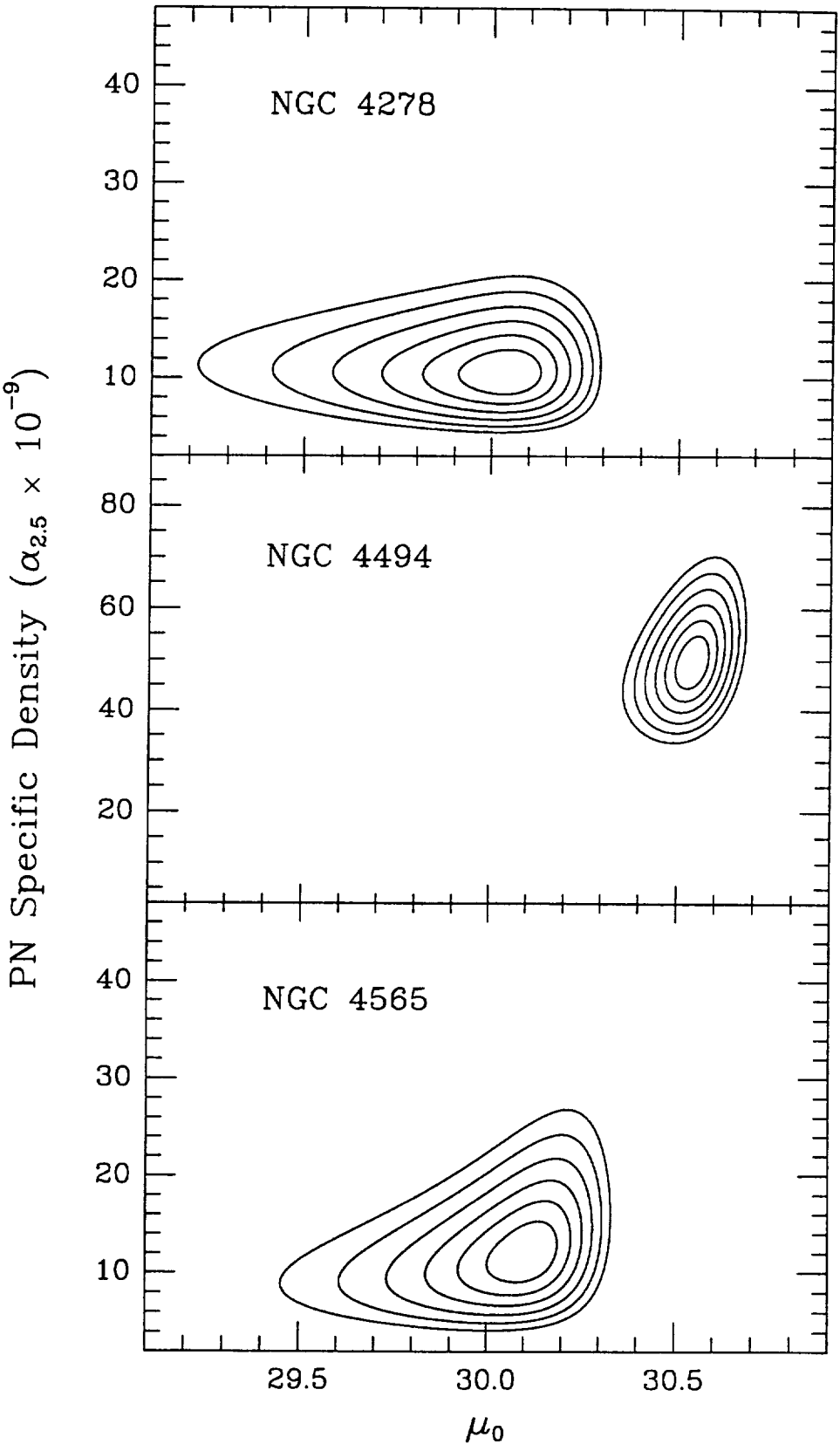

Fig. 4 - Jacoby et al

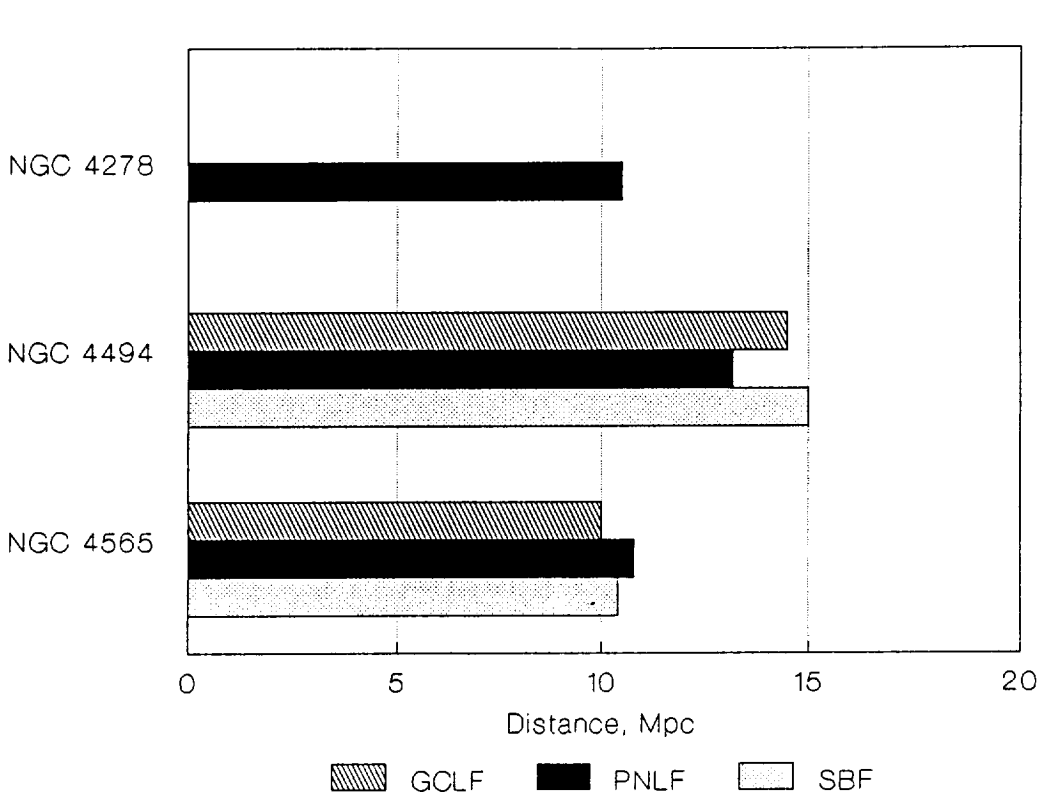

Fig 5 – Jacoby et al

N

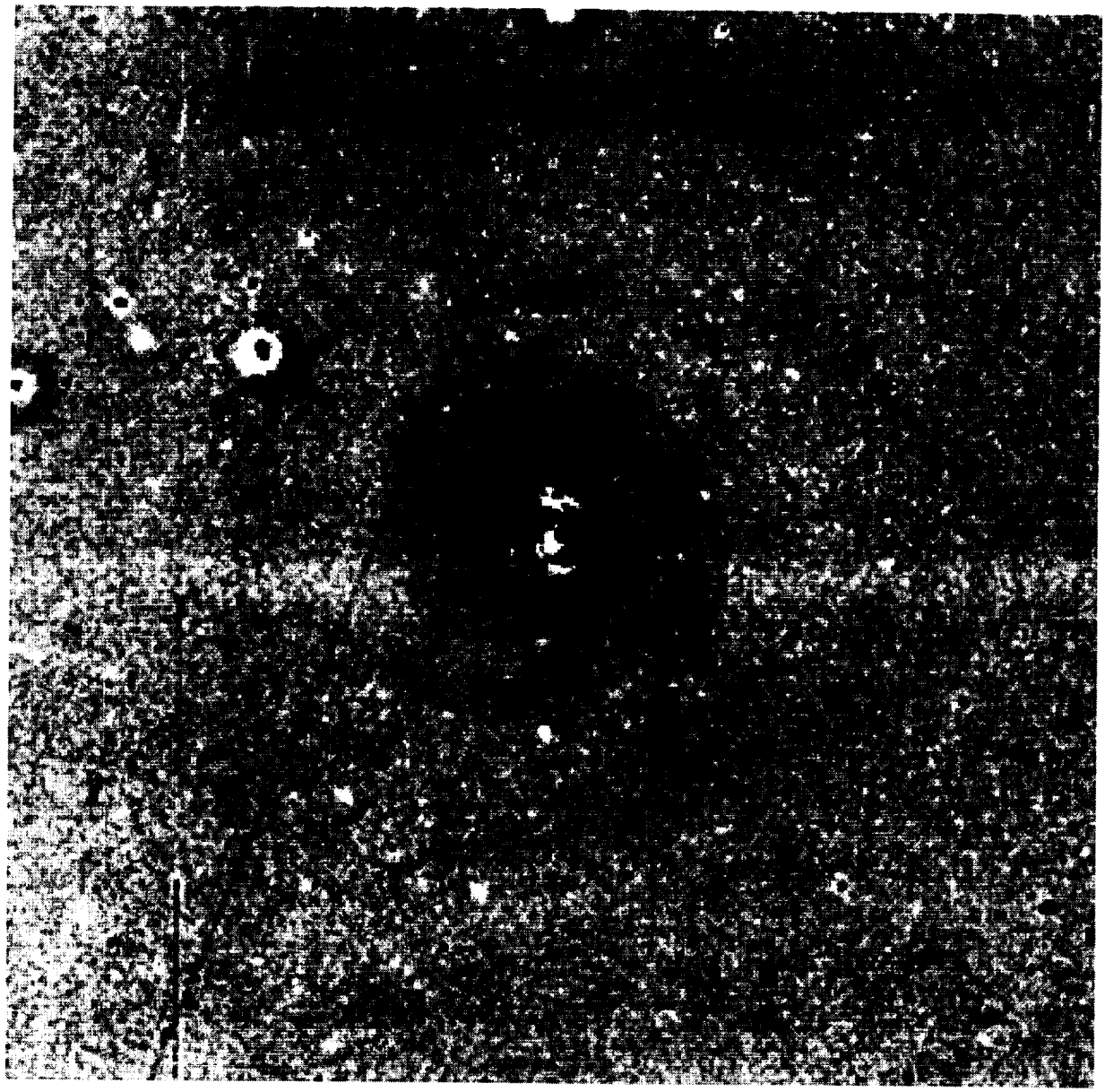

E

Figure 6- Jacobyetal